Silk Fiber Multiwalled Carbon Nanotube-Based Micro-/Nanofiber Composite as a Conductive Fiber and a Force Sensor

Sindhu Sree Muralidhar, Vinay Gangaraju, Mahesh Shastri, Navya Rani Marilingaiah, Arjun dey, Sushil Kumar Singh, and Dinesh Rangappa*

Read Online

ACCESS | Metrics & More | Article Recommendations | SI Supporting Information

ABSTRACT: Silk cocoon fibers (SFs) are natural polymers that are made up of fibroin protein. These natural fibers have higher mechanical stability and good elasticity properties. In this work, we coated multiwalled carbon nanotubes (MWCNTs) on the surface of SFs using a simple stirring technique with vinegar as the medium. This SF-MWCNT micro-/nanofiber composite was prepared without any adhesives. The characterization results revealed that the SF-MWCNT micro-/nanofiber composite exhibited excellent electrical conductivity (995 Ω cm^{-1}), tensile strength (up to 200% greater elongation), and durability characteristics. In addition, this micro-/nanofiber composite shows a change in resistance from 1450 to 960 Ω cm^{-1} for an applied mechanical force of 0.3−1 N kg^{-1}. Based on our findings, SF-MWCNT micro-/nanofiber composite-based conductive fibers (CFs) and force sensors (FSs) were developed.
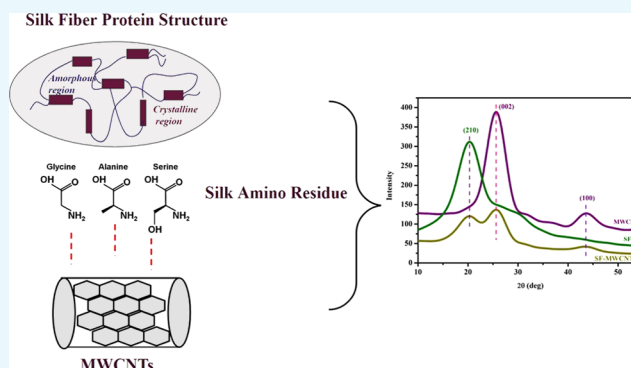
INTRODUCTION

Smart fabrics/textiles are the new-generation technology for material engineering.[1,2] Particularly, conductive fiber-based weaving technology for electronic fabrications such as sensors, circuits, batteries, and smart display systems has a wide range of textile applications.[3−5] To develop a conductive fiber, the fiber has to form a composite with a conductive material such as metal, carbon, and so on. In recent times, nanocomposites such as graphene, reduced graphene oxide, and carbon nanotubes[6−8] have been popularly used for fabricating conductive fibers. Although conductive fibers have the utmost advantage to be used for replacing synthetic materials with biomaterials, they still present the challenge of achieving excellent mechanical and electrical properties in one single fiber system.[9−11] For example, spider silk fiber MWCNT composite-based conductive fibers have been developed, which resulted in good electric conductivity, but they lack the stability and durability needed to meet textile requirements.[12]

Among many available natural polymers, our interest is invested in silk fibers (*Bombyx mori*) due to their excellent structural and functional properties, which are suitable to develop new devices for advanced applications. These fibers are smooth, flexible, lightweight, biodegradable, and available for large-scale production.[13−16] They have high mechanical stability and are tougher than metallic wires, carbonic threads, and Kevlar fibers.[17,18] However, despite these properties, silk fibers are extremely poor in conductivity; in fact, without treatment, these fibers are good insulators.

Considering their properties, researchers have reported various methods to develop conductive silk fibers. These included surface-coating technology (such as metal particles[19,20] and carbon graphene[21,22]), conductive polymer coating (e.g., polypyrrole[23,24]), carbonization of silk fibers,[25] and feeding silkworms with carbon nanomaterials.[26,27] Among nanocomposites, multiwalled carbon nanotube-based conductive fibers show high tensile strength and excellent conductivity.[19,20,27] In comparison, the carbonization of silk fiber and surface-coating have become effective approaches because of their good electrical conductivity.[28−30] However, both methods result in lower mechanical strength and toughness of the silk fiber due to excessive heat treatment for long hours to carbonize the silk fiber. Surface-coating techniques such as coating the silk fiber with metallic and polymer particles through a chemical route modify the surface of the fiber.[19,20] Due to this, a decrease in the electrochemical performance and degradation or fading of deposited particles occurs, resulting in a redoping process.

Cao et al. synthesized electrically conductive silk fibers using the electrostatic self-assembly method.[31−33] Here, silk fibers

are deposited with reduced graphene oxide (rGO) and polyaniline (PANI) conductive materials in an acid medium under high temperature. Although this method shows good electrical conductivity, it lowers the tensile strength, durability, and stability of the fiber. This is due to the treatment of the fiber in an acid medium, followed by high-heat treatment, which damage the structural properties of the fiber. Thus, obtaining superior mechanical stability and electrical conductivity in a single fiber remains a significant challenge.

Inspired by the chemical route to synthesize conductive silk fibers,[34−36] in this paper, we present the surface-coating of silk fibers with MWCNTs using a simple stirring method. Thus, silk cocoon fiber and multiwalled carbon nanotube (SF-MWCNT) micro-/nanofiber composites with good electrical conductivity and excellent mechanical strength were obtained, which can be used as conductive fibers. Furthermore, when physical force is applied to this micro-/nanofiber composite, its properties change, opening up the possibility of developing a force sensor to monitor mechanical operations. Thus, this material may lead to a wide range of applications in wearable devices, health monitoring, and stress−strain sensors.

2. MATERIALS AND METHODS

2.1. Materials. Silk fibers processed with four twisting lines were obtained from the central silk board (Bengaluru, India). Multiwalled carbon nanotubes (MWCNTs) were purchased from Nopo technologies (Bengaluru, India); they were 50 μm in length, with an average diameter of 8−10 nm, a carboxyl content of 2.56 wt %, and a carbon purity of more than 95 wt %. Vinegar was obtained by dissolving 5 wt % acetic acid in 500 mL of water. All chemicals are analytical grade and used without any further modification in this work.

2.2. Preparation of SF-MWCNT Fiber Composites. SF-MWCNT-based micro-/nanofiber composites were prepared using a simple stirring method with vinegar as the medium (graphical representation shown in Figure 1). The MWCNT
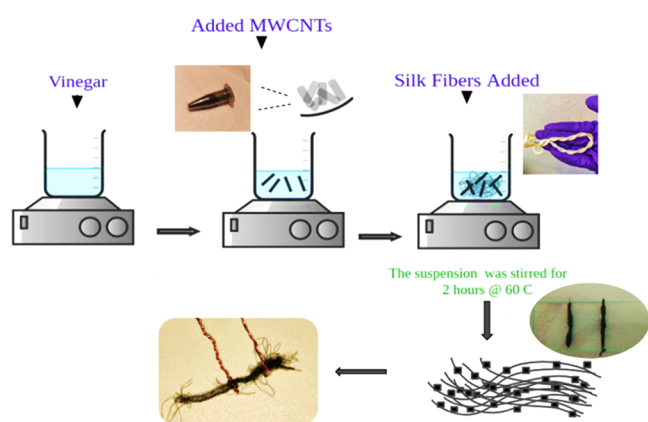
Figure 1. Graphical representation of the SF-MWCNT micro-/nanofiber composite synthesis process.

(2 mg) was dissolved in 30 mL of vinegar solution and stirred for 30 min. Afterward, silk fibers were added to the solution and stirred for 2 h at 60 °C. Here, a bunch of silk fibers (15 cm) with an average weight of 16 mg was used. Due to the static reaction and surface affinity of fibers, MWCNTs were deposited on the silk fibers. These fibers were extracted using tweezers and air-dried at room temperature. The as-prepared SF-MWCNT-based micro-/nanofiber composites were exam-

ined for their electrical conductivity and mechanical sensing properties.

2.3. Material Characterization. The surface morphology and elemental analyses of bare SFs and SF-MWCNT fibers were performed, respectively, by scanning electron microscopy (SEM, Hitachi SU1510) and EDAX (Thermo Fisher Scientific) after sputtering with gold. X-ray diffraction (XRD Rigaku IV) analysis of as-prepared samples was performed using Cu Kα1 radiation, with a 2θ diffraction angle of 10 to 80° with a step width of 0.02 at 35 kV and 25 mA. The surface functional group analysis was performed using Fourier transform infrared spectroscopy (PerkinElmer STA8000) and Raman spectroscopy (Xplora Horiba Scientific) at 400 to 4000 cm^{-1}. The elongation test was conducted using micro UTM (Mecmesin, CeNse Lab, IISC). An electrochemical workstation (Keithley 2400 SMU model) was employed to analyze the electrical characteristics.

3. RESULTS AND DISCUSSION

3.1. Morphological Analysis. The surface morphology of bare SFs and SF-MWCNT micro-/nanofiber composites were analyzed using SEM and are presented in Figure 2. A bare SF is milky white in color and has a smooth surface with a lustrous texture (Figure 2a−c). Generally, after a degumming process of the silk cocoon, 2 to 4 individual fibers are intertwined as a single fiber, which is known as reeling. This process was carried out to increase the stiffness and durability of the fiber.[37,38] Therefore, the bare SF consists of multiple fibers twisted together, thereby forming a porous structure in between them (Figure 2a,d). For all further analysis, these fibers are considered. After surface-coating, we observed the uniform deposition of MWCNTs on and in between the fibers at different magnifications, as shown in Figure 2g−i. This may be due to the MWCNT particle size being smaller than that of the silk fiber; the CNT might be filled into the subsurface of the bundle of silk fibrils, with either the cross or the antiparallel β-sheet structure being predominant, thereby confirming the possibility of a uniform coating throughout the fiber. Thus, the formation of SF-MWCNT micro-/nanofiber composites was confirmed. However, due to the rapid stirring process, some large particles of MWCNT deposited on the fiber surface were noticed (Figure 2l). The cross-sectional views of the bare SF and SF-MWCNT samples are shown in Figure 2d−f,j,k, respectively. It is evident that MWCNTs have been deposited at the ends of the fiber, thus confirming the distribution of nanotubes throughout the fiber.

Subsequently, EDAX analysis was performed for both bare SF and SF-MWCNT samples, as shown in Figure 3. From the EDAX analysis, the weight percentages (%) of different elements such as carbon (C), oxygen (O), and nitrogen (N) were analyzed. The obtained results clearly indicate an increase in the weight percentage of carbon after MWCNT deposition. This confirms the formation of SF-MWCNT micro-/nanofiber composites. For a better understanding, summarized results of bare SF and SF-MWCNT micro-/nanofiber composites are shown in Table 1. Along with this, the presence of other elements such as nitrogen, oxygen, sodium, and potassium is noticed, which is also in agreement with published reports.[39]

3.2. Structural Analysis. The XRD analysis was performed on bare SFs and SF-MWCNT micro-/nanofiber composites to identify their crystal structure, and the results are shown in Figure 4. The XRD pattern of the pristine MWCNT sample shows diffraction peaks at 2θ = 25.64 and
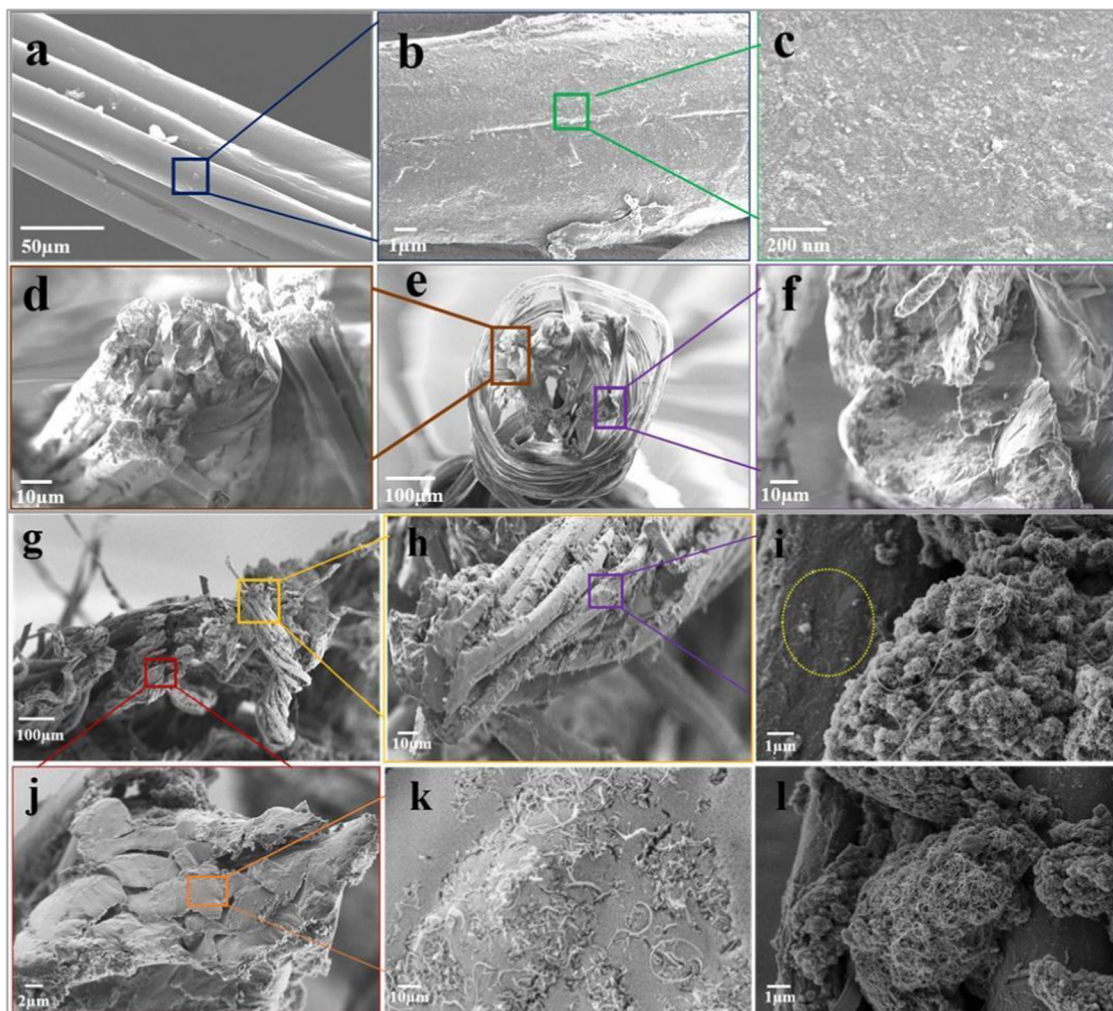
Figure 2. SEM images of SF and SF-MWCNT samples: (a−c) SF fiber surface; (d−f) cross-sectional view of SF fibers; (g−i) SF-MWCNT micro-/nanofiber composite with a surface-coating of MWCNTs throughout the fiber and (j−l) cross-sectional view of the SF-MWCNT micro-/nanofiber composite.
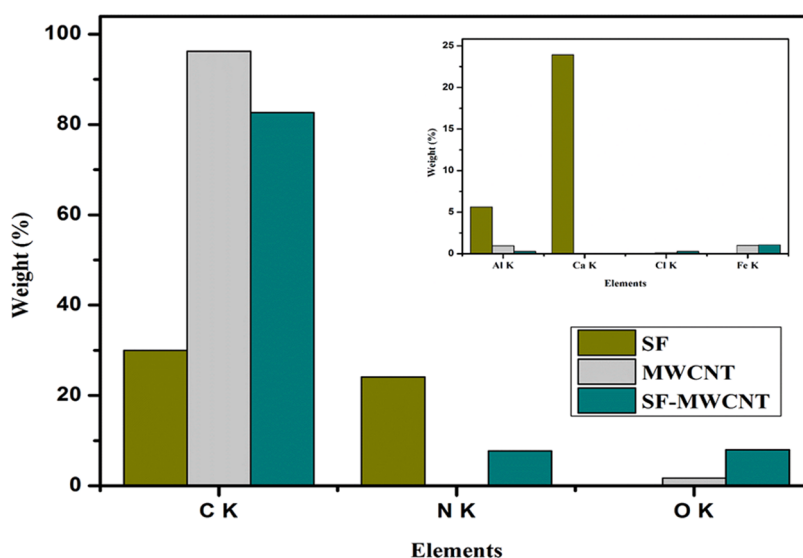
Figure 3. Elemental (EDAX) analysis of MWCNT (gray), SF (dark yellow), and SF-MWCNT (cyan) samples.

43.60°, which correspond to the (002) and (100) planes of the MWCNT, respectively.[39,40] However, the XRD pattern of bare

SF has a diffraction peak at $2\theta = 20.32°$, which represents the β-sheet crystal structure with the (210) plane of the silk

Table 1. Elemental Analysis of MWCNT, SF, and SF-MWCNT samples by EDAX Showing the Composition in Weight Percentage (%)

elements	MWCNT weight (%)	SF weight (%)	SF-MWCNT weight (%)
carbon (C K)	96.23	29.99	82.64
nitrogen (N K)	0	24.09	7.75
oxygen (O K)	1.69	16.38	7.98
aluminum (Al K)	0.96	5.62	0.28
calcium (Ca K)	0	23.92	0
chlorine (Cl K)	0.1	0	0.28
iron (Fe K)	1.01	0	1.07
total	99.99	100	100
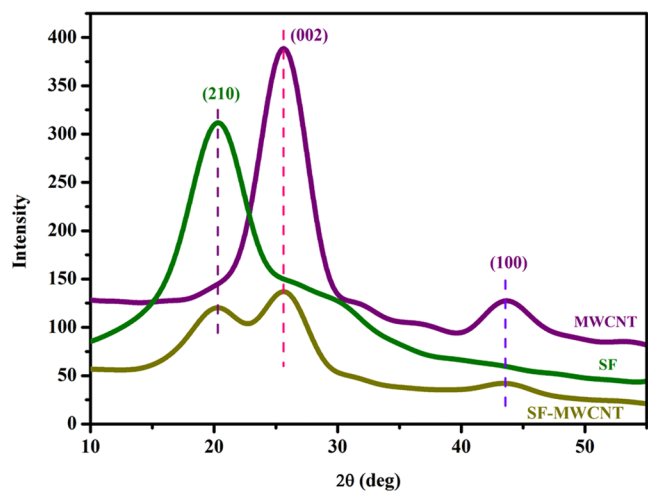
Figure 4. XRD patterns of the pristine MWCNT, silk fiber, and SF-MWCNT samples prepared by a simple stirring method.

fiber.[41−44] Generally, the secondary protein structure of silk cocoon fibers consists of an α-helix (amorphous region) with the (110) plane, β-sheet (crystalline region) with the (210) plane, and a random coil with the (020) plane, respectively. Here, during the pre-process (reeling) of SFs, the α helix and random coil, which are weak hydrophilic bonds, are removed easily. Hence, the absence of the (110) and (020) planes is observed in the XRD pattern of Figure 4. The peaks at 20.32, 25.64, and 43.60° confirm the formation of SF-MWCNT micro-/nanofiber composites. From the analysis, it is clearly noticed that after the deposition of MWCNTs, there is a slight decrease in the intensity of bare SF, which corresponds to a decrease in the percent crystallinity from 5.94 to 2.96%.[38,45] This may be due to the fact that the deposition of MWCNTs on SF has modified the surface. However, MWCNTs did not affect the β-sheet crystal structure of the fiber as evidenced by the XRD pattern of the SF-MWCNT fiber composite. This is a significant fact because the presence of the β-sheet shows the stability of the fiber.[46]

The functional group analysis of both bare SF and SF-MWCNT fiber composites was performed using FTIR spectroscopy in the range of 400−4000 cm^{-1}, as shown in Figure 5. Functional group peaks of the bare SF and SF-MWCNT fiber composite are shown in Figure 5a,b, respectively. Silk fibers possess two structural models: α helix as Silk I and β-sheet as Silk II. The amide I (−CO− and −CN−stretching) in the region of 1655−1660 cm^{-1}, amide II (−NH− bending) in the region of 1531−1542 cm^{-1}, and amide III (−CN− stretching) in the region of 1230 cm^{-1} belonged to the Silk I conformation.[45−47] Similarly, infrared absorption peaks of Silk II in amides I, II, and III were observed at 1620−1630, 1515−1530, and 1240 cm^{-1} respectively, and random coils occurred at 1640−1648, 1535−1545, and 1235 cm^{-1}, respectively.[27,45−47] Hence, no significant difference was found in the fingerprint region. This confirms the presence of a β-sheet crystal structure, and hence, the results are in agreement with the XRD patterns observed. However, the C-OH group observed at 2856 and 2971 cm^{-1} regions in the bare SF sample disappeared in SF-MWCNT fiber composite samples. This may be due to the interaction of MWCNTs with the backbone hydrogen chain of the fiber protein structure. Similar changes were reported by Steven et al., wherein spider silk was amine-functionalized with multi-walled carbon nanotubes, and they reported changes in the O−H and C−H groups of the fiber after functionalization.[12] For
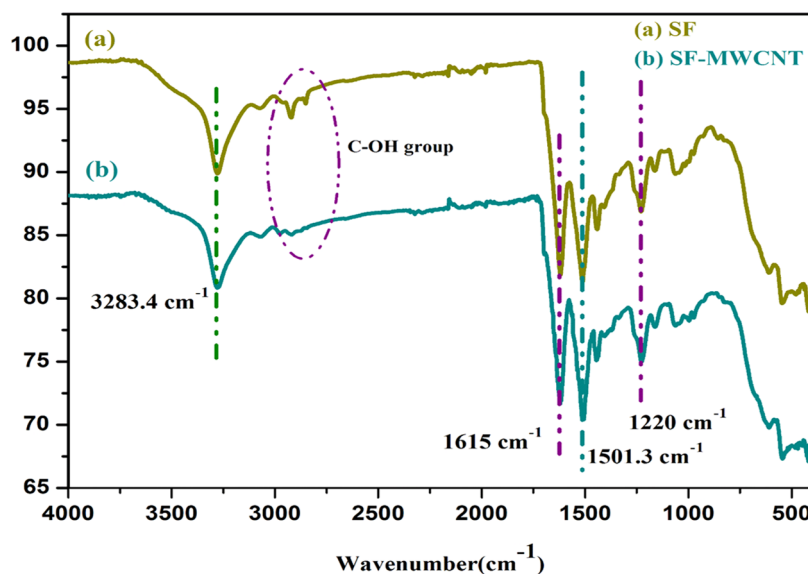
Figure 5. FTIR spectra of (a) silk fiber and (b) SF-MWCNT samples after the deposition of MWCNTs by a simple stirring method.
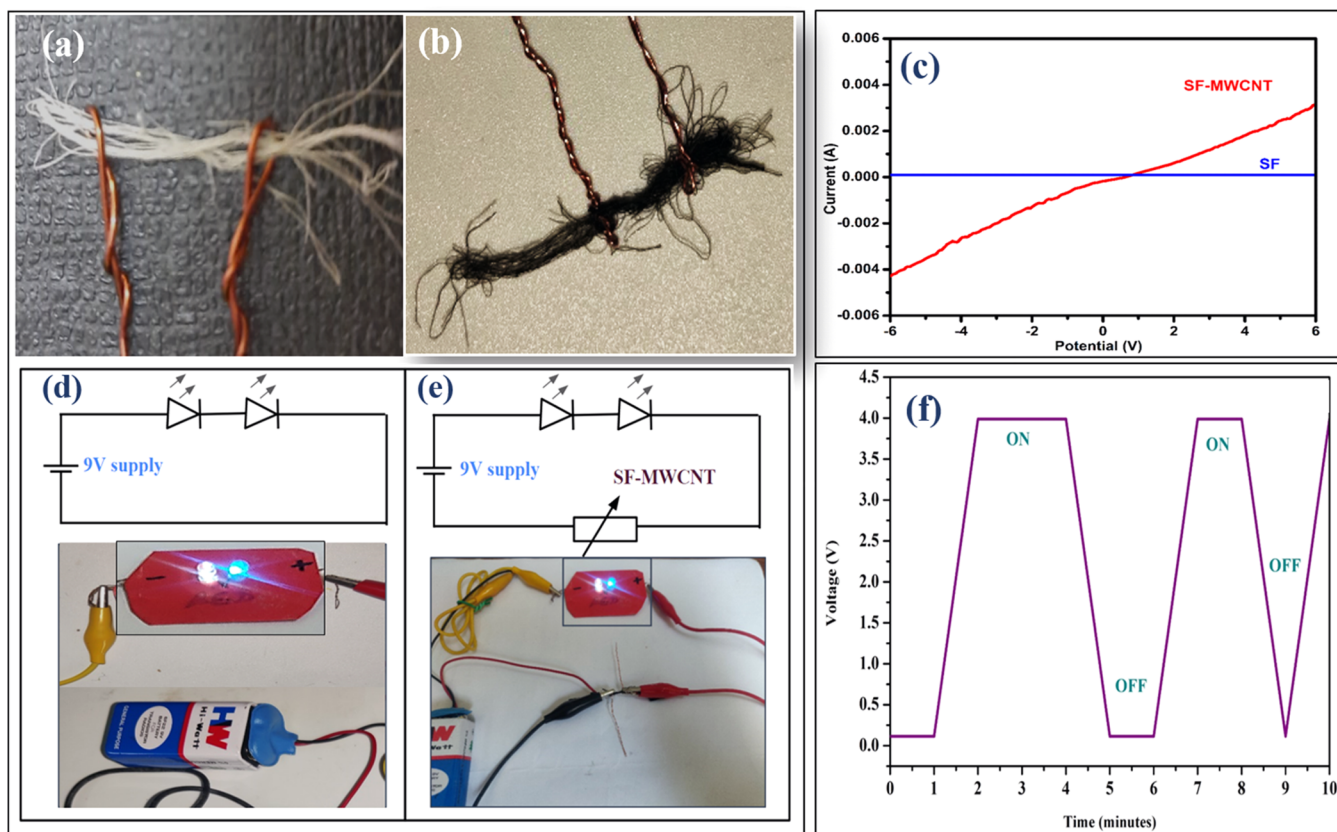
Figure 6. Electrical characteristics of SF and SF-MWCNT: (a) photograph of SF and (b) SF-MWCNT with electrical contacts used for electrical measurement; (c) I−V characteristics of SF and SF-MWCNT in the voltage window of −10 to 10 V; (d) LED lights lit up with a normal electrical wire at 9 V; (e) LED lights lit up through an SF-MWCNT micro-/nanofiber composite conductive wire connection (inset image: highlighting the fiber composite connection); and (f) switching capacity of SF-MWCNT micro-/nanofiber composites.
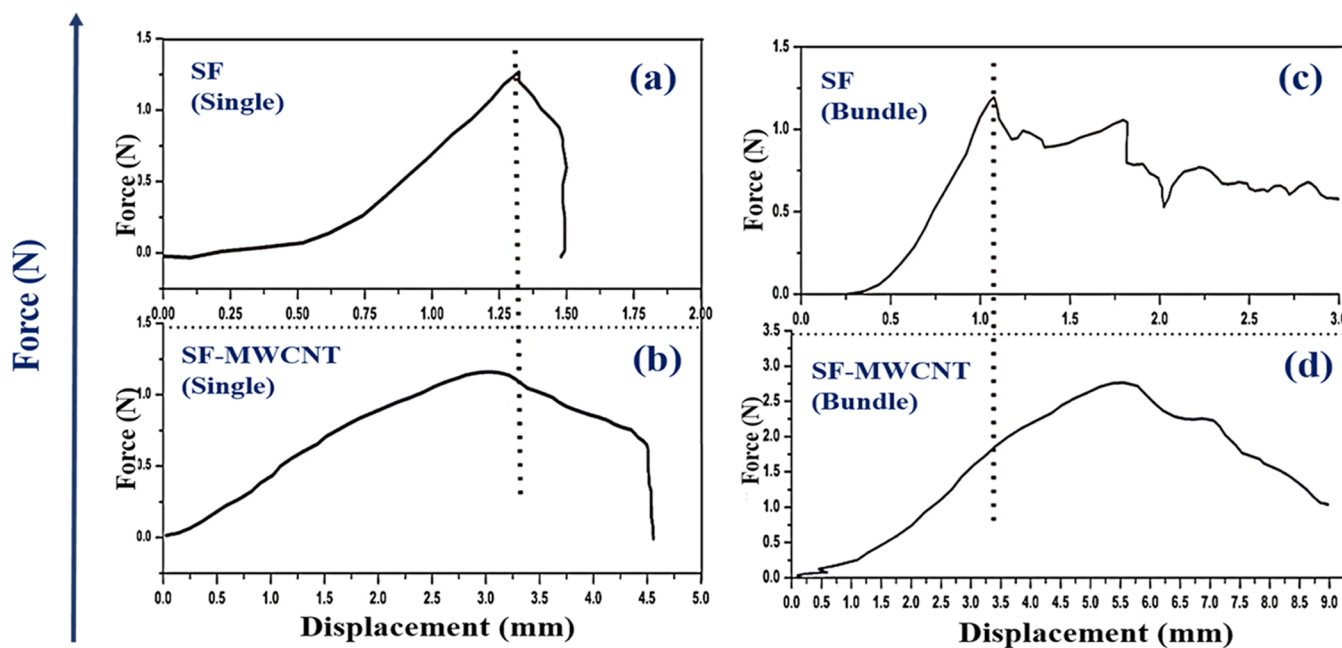
Figure 7. Tensile strength analysis of (a, b) single fibers of bare SF and the SF-MWCNT fiber composite and (c, d) bundle fibers of bare SFs and the SF-MWCNT fiber composite.

further confirmation, we obtained the Raman spectra for MWCNT, SF, and SF-MWCNT, and the results showed the formation of the fiber composite, as shown in Figure S1.

3.3. Electrical Characteristics. The electrical conductivities of the bare SF and SF-MWCNT micro-/nanofiber composite were evaluated using knotted SF samples with a
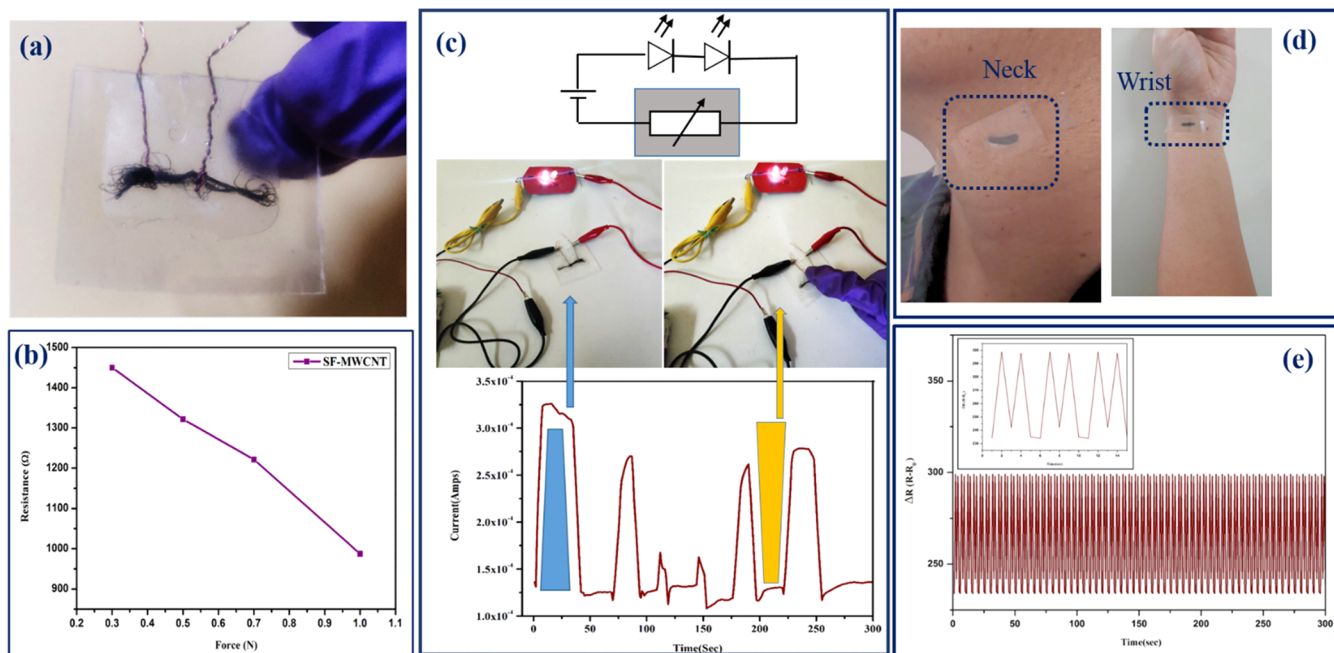
Figure 8. Change in the resistance of the SF and SF-MWCNT fibers with respect to force: (a) SF-MWCNT fiber model sealed along with electrical contacts; (b) change in the resistance for an applied force of 0.3−1 N kg^{-1}; (c) contrasting behavior, with a decrease in the current density when the force was applied with respect to the load; (d) photograph of the pulse frequency measurement of the wrist and neck; and (e) change in the total conductance ΔR with respect to the pulse frequency of the wrist.

single-stranded copper wire (Figure 6a,b) to establish electrical contact. An $I−V$ analysis was carried out in the voltage range of −5 to 5 V to study its subsequent current response, and the results are presented in Figure 6c. It was observed that bare SF did not generate current with respect to the voltage applied as bare SF has a high resistance due to its insulating nature.[48] However, SF-MWCNT shows the generation of a current of up to 2 mA, indicating that the MWCNT deposition converted the SF into conducting fibers. This may be due to the alignment of the MWCNTs on the polymer substrate forming a conducting path throughout the length of the fiber.[12,49−51] Hence, the composited fiber shows a higher conductivity and continuity compared with bare SF; therefore, SF-MWCNT composites were subjected to further analyses. In addition, an electricity conductivity of up to 995 Ω cm^{-1} or 9.95 S m^{-1} was achieved using the simple stirring method. Table S1 shows a summary of studies that reported on various polymers coated with carbonaceous materials such as CNTs. Carbon black has been reported to exhibit an electrical conductivity ranging from 3.1×10^4 to 12.6 S m^{-1}. Thus, based on the findings, this method has shown a higher electrical conductivity than those with other CNT-functionalized polymers.

Subsequently, the SF-MWCNT fiber was tested as a conductive fiber (CF) to light up two LEDs (3 V each) that were connected in series. These LEDs lit up when a 9 V input voltage was applied, as shown in Figure 6d. Then, two LEDs were connected in series with the SF-MWCNT composite and they also lit up for the same input voltage (Figure 6e). This proves that the fiber composite has good electrical conductivity and its interlayer-like arrangement facilitates the flow of electrons or ions in the fiber.[51−53] Further, we also analyzed the switching response (rapidly changing input supply from the On to the Off state and vice versa) of the fiber composite and observed no electrical current loss during the process (Figure 6f). Based on the results, it is suggested that the fiber

composite synthesized via the stirring method can be used as a conductive fiber.

3.4. Tensile Strength Characteristics. The tensile strength of the fibers was evaluated by a force−displacement curve analysis of the bare SF and SF-MWCNT micro-/nanofiber composite using a single fiber and a bundle of fibers (20 fibers), as shown in Figure 7. Figure 7a,b, shows the elongation strength of a single bare SF and the SF-MWCNT fiber, respectively. It was observed that both the fibers support a loading capacity of up to 1.5 N, and it was evident that the SF-MWCNT composite had a greater elongation of about 200% compared with bare SF fibers. Further, the elongation strength of a bundle (20 fibers) of SF and SF-MWCNT fibers was investigated, as shown in Figure 7c,d. It is obvious that with the addition of fibers, the loading capacity increases as multiple fibers overcome the friction loss associated with a single fiber. It is noticeable that for a bundle of SF-MWCNT fibers, the loading capacity increased up to 3 N compared with bare SF fibers. Based on our findings, it is concluded that the elongation strength of silk fibers increased after the deposition of MWCNTs. Naturally, SFs possess a higher tensile strength due to the presence of the β-sheet protein. However, with the addition of MWCNTs, the tensile strength of SFs was further increased. Due to this, the addition of MWCNTs influences the molecular kinetics of the fiber and improves its mechanical properties.[49,54,55] Figure S2 shows the SEM morphology of the elongated single bare SF and SF-MWCNT fiber composite after being influenced by a loading capacity of 1.5 N. It is visually observed that the SF-MWCNT fiber composite has fewer breaks compared with bare SF.

Figure S3 shows the thermogravimetric analysis (TGA) thermolysis curve of the SF and SF-MWCNT micro-/nanofiber composite samples measured over a temperature range of 50 to 350 °C. It was observed that the presence or absence of an MWCNT coating did not cause a significant
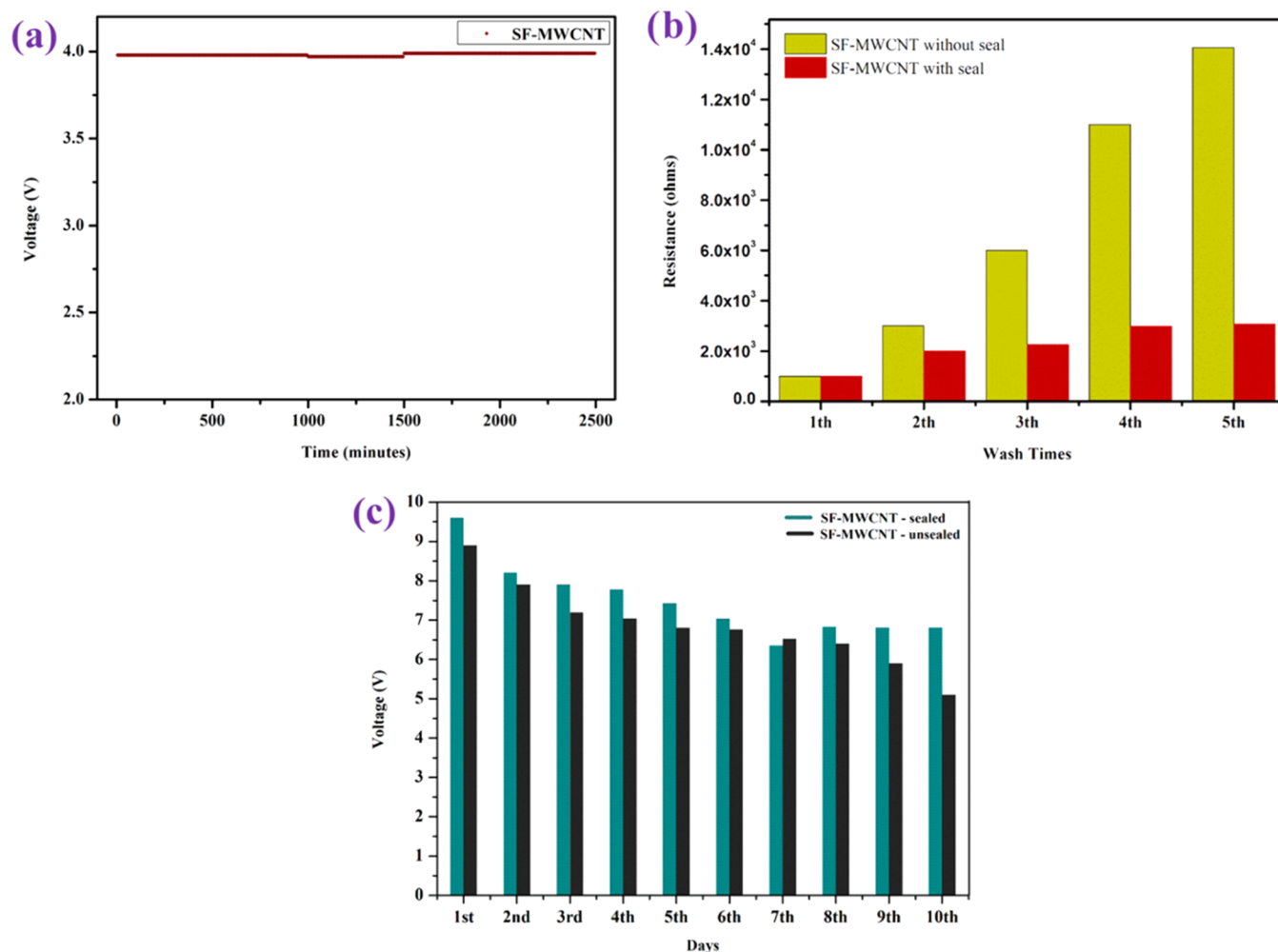
Figure 9. Durability analysis of the SF-MWCNT micro-/nanofiber composite: (a) voltage drop across the fiber composite tested over 41.6 h; (b) resistance change after washing fibers five times; and (c) material degradation analysis for 10 days.

change in the thermolysis of the SF and SF-MWCNT fiber composite samples, which indicates that no deterioration of the β-sheet occurred after the addition of MWCNTs, and hence, the results are in agreement with the XRD, FTIR, and tensile strength patterns observed.

3.5. Force Analysis. We noticed a change in the resistance when a force was applied to the SF-MWCNT fiber composite. Figure 8 shows the force sensor (FS) property of the SF-MWCNT fiber composite. Here, the fiber composite was sealed along the electrical contacts using a laminated sheet, as shown in Figure 8a. The change in resistance was noticed for an applied force of 0.3−1 N kg^{-1}. With an increase in the force input, a decrease in the resistance was observed, as shown in Figure 8b. This behavior is possible because on stretching the composite fiber, the distribution of MWCNTs throughout the fiber increases, thereby causing a decrease in the electrical resistance. After the release of the force, the fiber returns to its initial resistance.[49,54,55]

A contrasting behavior was noticed when the same fiber was connected to an input supply (9 V) where a decrease in the current occurred when a force was applied, which is visibly evident with the decrease in the intensity of LED lights, as shown in Figure 8c. For a better understanding, we simultaneously measured the change in the current density of the LEDs without and with force input, as shown in Figure

8c, and noticed the same behavior. This is due to the fact that when a force was applied to the fiber composite, a disruption in the charge flow occurred, resulting in a decrease in the current.[56]

Our curiosity led us to analyze these micro-/nanofiber composite-based force sensors for detecting the pulse frequency when connected to either the neck or the wrist (Figure 8d). The change in the total resistance (ΔR) was plotted with respect to time (Figure 8e) for the detection of the wrist pulse frequency, and we noticed a frequent change in resistance for the corresponding wrist pulse frequency. For a confirmation, we also analyzed the behavior of the SF-MWCNT fiber when no physical force/pressure was applied and observed no change in the resistance (Figure S4). Here, the total resistance (ΔR) is calculated as follows:[12,51]

$$\Delta R = R - R_0$$

where the resistance of a fiber measured without any physical input is considered as the initial resistance (R_0) and the resistance with respect to the force/applied pressure is considered as the measured resistance R. Further, for the same fiber composite (Figure 8a), we analyzed the electrical conductivity characteristics and found a continuous conductivity with no electrical loss, as shown in Figure S5.

3.6. Durability Analysis. The durability of the SF-MWCNT fiber composite was examined under three conditions: (1) during a voltage drop across the fiber with respect to time; (2) after washing the fiber several times; and (3) after material degradation when exposed to the environment (Figure 9). Here, a voltage window of 0−5 V was applied as an input supply. Figure 9a shows a lower voltage drop across the fiber composite over a period of 2500 min (41.6 h) and hence confirms that there is continuous conduction without any deterioration in the composite. Further, we analyzed the resistance of the fiber composite after washing five times (Figure 9b) with normal water. For a better understanding, we noted the change in the resistance in the absence and presence of a laminated seal on SF-MWCNT fibers. It was observed that the variation in the resistance of the SF-MWCNT fiber without a laminated seal (1−14 kΩ cm^{-1}) was much higher than that of the SF-MWCNT micro-/nanocomposite fibers with a laminated seal. Thus, it proved that the simple fabrication method led to a better durability of the fiber composite .

In addition, Figure 9c shows the voltage change when the fiber composite was exposed to the environment for 10 days in the presence and absence of a laminated seal on SF-MWCNT fibers. We monitored their degradation rates with respect to a constant input voltage (10 V) when exposed to the environment. It is evident that sealed SF-MWCNT fibers have a lower degradation than unsealed fibers. Thus, based on our findings, sealed SF-MWCNT fiber composites showed resistance to external conditions such as water wash and exposure to the environment.

4. CONCLUSIONS

In conclusion, an efficient and simple stirring technique was developed to coat MWCNTs on the surface of SFs without using any adhesives. SF-MWCNT micro-/nanofiber composites with an electrical conductivity of 995 Ω cm^{-1} and a high mechanical strength were achieved. The prepared micro-/nanofiber composites were developed as conductive fibers (CFs) and force sensors (FSs). The mechanical properties of the SF-MWCNT fibers included an excellent tensile strength with the highest loading capacity of up to 3 N and 200% elongation capacity compared with bare SFs. Further, the fiber composite sealed with a laminated sheet showed resistance to external conditions such as water wash and exposure to the environment and provided a simple fabrication method to protect the fibers from damage. This work demonstrated good electrical conductivity and high mechanical stability in one single fiber that can be used for e-textiles, biomedical sensors, MEMS/NEMS, and wearable electronic applications.

ASSOCIATED CONTENT

Ⓢ Supporting Information

The Supporting Information is available free of charge at https://pubs.acs.org/doi/10.1021/acsomega.2c01392.

> Raman spectra of the MWCNT and SF-MWCNT; SEM morphological analysis of bare SF and SF-MWCNT fibers after elongation up to 1.5 N; TGA curve pattern of SF and SF-MWCNT; resistance vs time analysis of SF-MWCNT fibers when no physical force was applied; electrical conductivity prototype of sealed SF-MWCNT; summarized report of electrical conductivity of various polymers (PDF)

AUTHOR INFORMATION

Corresponding Author

Dinesh Rangappa − *Department of Applied Sciences, Visvesvaraya Technological University, Center for Postgraduate Studies, Bengaluru 562 101, India;* ⓞ orcid.org/0000-0001-7756-0266; Email: dineshrangappa@gmail.com

Authors

Sindhu Sree Muralidhar − *Department of Applied Sciences, Visvesvaraya Technological University, Center for Postgraduate Studies, Bengaluru 562 101, India*

Vinay Gangaraju − *Department of Applied Sciences, Visvesvaraya Technological University, Center for Postgraduate Studies, Bengaluru 562 101, India*

Mahesh Shastri − *Department of Electronics and communications, Nagarjuna College of Engineering and Technology, Devanahalli 562110, India*

Navya Rani Marilingaiah − *Department of Applied Sciences, Dayanand Sagar University, Bengaluru 560111, India*

Arjun dey − *Thermal Systems Group, ISRO Satellite Centre, Bangalore 560017, India*

Sushil Kumar Singh − *Acoustic Sensor Division, Solid State Physics Laboratory, Defence Research Development Organization (DRDO), New Delhi 110054, India*

Complete contact information is available at:
https://pubs.acs.org/10.1021/acsomega.2c01392

Notes

The authors declare no competing financial interest.

REFERENCES

(1) Ren, J.; Wang, Y.; Yao, Y.; Wang, Y.; Fei, X.; Qi, P.; Lin, S.; L Kaplan, D.; J Buehler, M.; Ling, S. Biological Material Interfaces as Inspiration for Mechanical and Optical Material Designs. *Chem. Rev.* **2019**, *119*, 12279−12336.

(2) Boulet-Audet, M.; Holland, C.; Gheysens, T.; Vollrath, F. Dry-Spun Silk Produces Native-Like Fibroin Solutions. *Biomacromolecules* **2016**, *17*, 3198−3204.

(3) Yang, W.; Yu, J.; Xi, X.; Sun, Y.; Shen, Y.; Yue, W.; Zhang, C.; Jiang, S. Preparation of Graphene/ITO Nanorod Metamaterial/U-Bent-Annealing Fiber Sensor and DNA Biomolecule Detection. *Nanomaterials* **2019**, *9*, 1154.

(4) Jang, Y.; Kim, S. M.; Spinks, G. M.; Kim, S. J. Carbon Nanotube Yarn for Fiber-Shaped Electrical Sensors, Actuators, and Energy Storage for Smart Systems. *Adv. Mater.* **2020**, *32*, No. 1902670.

(5) Smith, R. E.; Totti, S.; Velliou, E.; Campagnolo, P.; Hingley-Wilson, S. M.; Ward, N. I.; Varcoe, J. R.; Crean, C. Development of a Novel Highly Conductive and Flexible Cotton Yarn for Wearable PH Sensor Technology. *Sens. Actuators, B* **2019**, *287*, 338−345.

(6) Zeng, W.; Shu, L.; Li, Q.; Chen, S.; Wang, F.; Tao, X. M. Fiber-Based Wearable Electronics: A Review of Materials, Fabrication, Devices, and Applications. *Adv. Mater.* **2014**, *26*, 5310−5336.

(7) Heo, J. S.; Eom, J.; Kim, Y. H.; Park, S. K. Recent Progress of Textile-Based Wearable Electronics: A Comprehensive Review of Materials, Devices, and Applications. *Small* **2018**, *14*, No. 1703034.

(8) Agcayazi, T.; Chatterjee, K.; Bozkurt, A.; Ghosh, T. K. Flexible Interconnects for Electronic Textiles. *Adv. Mater. Technol.* **2018**, *3*, No. 1700277.

(9) Jalili, R.; Razal, J. M.; Wallace, G. G. Exploiting High Quality PEDOT:PSS-SWNT Composite Formulations for Wet-Exploiting High Quality PEDOT:PSS-SWNT Composite Formulations for Wet-Spinning Multifunctional Fibers Spinning Multifunctional Fibers. *J. Mater. Chem.* **2012**, *22*, 25174−25182.

(10) Wang, C.; Xia, K.; Zhang, M.; Jian, M.; Zhang, Y. An All-Silk-Derived Dual-Mode E-Skin for Simultaneous Temperature−Pressure Detection. *ACS Appl. Mater. Interfaces* **2017**, *9*, 39484−39492.

(11) Tang, Z.; Jia, S.; Wang, F.; Bian, C.; Chen, Y.; Wang, Y.; Li, B. Highly Stretchable Core−Sheath Fibers via Wet-Spinning for Wearable Strain Sensors. *ACS Appl. Mater. Interfaces* **2018**, *10*, 6624−6635.

(12) Steven, E.; Saleh, W. R.; Lebedev, V.; Acquah, S. F. A.; Laukhin, V.; Alamo, R. G.; Brooks, J. S. Carbon Nanotubes on a Spider Silk Scaffold. *Nat. Commun.* **2013**, *4*, No. 2435.

(13) Yarger, J. L.; Cherry, B. R.; Van Der Vaart, A. Uncovering the Structure-Function Relationship in Spider Silk. *Nat. Rev. Mater.* **2018**, *3*, No. 18008.

(14) Keten, S.; Xu, Z.; Ihle, B.; Buehler, M. J. Nanoconfinement Controls Stiffness, Strength and Mechanical Toughness of β-Sheet Crystals in Silk. *Nat. Mater.* **2010**, *9*, 359−367.

(15) Vepari, C.; Kaplan, D. L. Silk as a Biomaterial. *Prog. Polym. Sci.* **2007**, *32*, 991−1007.

(16) Hardy, J. G.; Scheibel, T. R. Composite Materials Based on Silk Proteins. *Prog. Polym. Sci.* **2010**, *35*, 1093−1115.

(17) Ling, S.; Kaplan, D. L.; Buehler, M. J. Nanofibrils in Nature and Materials Engineering. *Nat. Rev. Mater.* **2018**, *3*, No. 18016.

(18) Ling, S.; Chen, W.; Fan, Y.; Zheng, K.; Jin, K.; Yu, H.; Buehler, M. J.; Kaplan, D. L. Biopolymer Nanofibrils: Structure, Modeling, Preparation, and Applications. *Prog. Polym. Sci.* **2018**, *85*, 1−56.

(19) Ling, S.; Wang, Q.; Zhang, D.; Zhang, Y.; Mu, X.; Kaplan, D. L.; Buehler, M. J. Integration of Stiff Graphene and Tough Silk for the Design and Fabrication of Versatile Electronic Materials. *Adv. Funct. Mater.* **2018**, *28*, No. 1705291.

(20) Ayutsede, J.; Gandhi, M.; Sukiraga, S.; Ye, H.; Hsu, C. M.; Gogotsi, Y.; Ko, F. Carbon Nanotube Reinforced *Bombyx Mori* Silk Nanofibers by the Electrospinning Process. *Biomacromolecules* **2006**, *7*, 208−214.

(21) Chiu, W. T.; Chen, C. Y.; Chang, T. F. M.; Hashimoto, T.; Kurosu, H.; Sone, M. Ni−P and TiO2 Codeposition on Silk Textile via Supercritical CO2 Promoted Electroless Plating for Flexible and Wearable Photocatalytic Devices. *Electrochim. Acta* **2019**, *294*, 68−75.

(22) Zhou, J.; Zhao, Z.; Hu, R.; Yang, J.; Xiao, H.; Liu, Y.; Lu, M. Multi-Walled Carbon Nanotubes Functionalized Silk Fabrics for Mechanical Sensors and Heating Materials. *Mater. Des.* **2020**, *191*, No. 108636.

(23) Cucchi, I.; Boschi, A.; Arosio, C.; Bertini, F.; Freddi, G.; Catellani, M. Bio-Based Conductive Composites: Preparation and Properties of Polypyrrole (PPy)-Coated Silk Fabrics. *Synth. Met.* **2009**, *159*, 246−253.

(24) Malhotra, U.; Maity, S.; Chatterjee, A. Polypyrrole-Silk Electro-Conductive Composite Fabric by in Situ Chemical Polymerization. *J. Appl. Polym. Sci.* **2015**, *132*, No. 41336.

(25) Wang, Q.; Wang, C.; Zhang, M.; Jian, M.; Zhang, Y. Feeding Single-Walled Carbon Nanotubes or Graphene to Silkworms for Reinforced Silk Fibers. *Nano Lett.* **2016**, *16*, 6695−6700.

(26) Lepore, E.; Bonaccorso, F.; Bruna, M.; Bosia, F.; Taioli, S.; Garberoglio, G.; Ferrari, A. C.; Pugno, N. M. Silk Reinforced with Graphene or Carbon Nanotubes Spun by Spiders. 2015, arXiv:physics/1504.06751. arXiv.org e-Print archive. https://doi.org/10.48550/arXiv.1504.06751.

(27) Zhou, J.; Zhao, Z.; Hu, R.; Yang, J.; Xiao, H.; Liu, Y.; Lu, M. Multi-Walled Carbon Nanotubes Functionalized Silk Fabrics for Mechanical Sensors and Heating Materials. *Mater. Des.* **2020**, *191*, No. 108636.

(28) Wang, C.; Xia, K.; Jian, M.; Wang, H.; Zhang, M.; Zhang, Y. Carbonized Silk Georgette as an Ultrasensitive Wearable Strain Sensor for Full-Range Human Activity Monitoring. *J. Mater. Chem. C* **2017**, *5*, 7604−7611.

(29) Wang, C.; Li, X.; Gao, E. L.; Jian, M. Q.; Xia, K. L.; Wang, Q.; Xu, Z. P.; Ren, T. L.; Zhang, Y. Y. Carbonized Silk Fabric for Ultrastretchable, Highly Sensitive, and Wearable Strain Sensors. *Adv. Mater.* **2016**, *28*, 6640−6648.

(30) Chen, C.; Ran, R.; Yang, Z.; Lv, R.; Shen, W.; Kang, F.; Huang, Z. H. An Efficient Flexible Electrochemical Glucose Sensor Based on Carbon Nanotubes/Carbonized Silk Fabrics Decorated with Pt Microspheres. *Sens. Actuators, B* **2018**, *256*, 63−70.

(31) Ma, D. L.; Ma, Y.; Chen, Z. W.; Hu, A. M. A Silk Fabric Derived Carbon Fibre Net for Transparent Capacitive Touch Pads and All-Solid Supercapacitors. *J. Mater. Chem. A* **2017**, *5*, 20608−20614.

(32) Chen, C. Y.; Huang, S. Y.; Wan, H. Y.; Chen, Y. T.; Yu, S. K.; Wu, H. C.; Yang, T. I. Electrospun Hydrophobic Polyaniline/Silk Fibroin Electrochromic Nanofibers with Low Electrical Resistance. *Polymers* **2020**, *12*, 2102.

(33) Cao, J.; Huang, Z.; Wang, C. Natural Printed Silk Substrate Circuit Fabricated via Surface Modification Using One Step Thermal Transfer and Reduction Graphene Oxide. *Appl. Surf. Sci.* **2018**, *440*, 177−185.

(34) Zhang, F.; Lu, Q.; Ming, J.; Dou, H.; Liu, Z.; Zuo, B.; Qin, M.; Li, F.; Kaplan, D. L.; Zhang, X. Silk Dissolution and Regeneration at the Nanofibril Scale. *J. Mater. Chem. B* **2014**, *2*, 3879−3885.

(35) Phillips, D. M.; Drummy, L. F.; Conrady, D. G.; Fox, D. M.; Naik, R. R.; Stone, M. O.; Trulove, P. C.; De Long, H. C.; Mantz, R. A. Dissolution and Regeneration of *Bombyx Mori* Silk Fibroin Using Ionic Liquids. *J. Am. Chem. Soc.* **2004**, *126*, 14350−14351.

(36) Kweon, H.; Park, Y. H. Dissolution and Characterization of Regenerated Antheraea Pernyi Silk Fibroin. *J. Appl. Polym. Sci.* **2001**, *82*, 750−758.

(37) Zhao, H. P.; Feng, X. Q.; Shi, H. J. Variability in Mechanical Properties of *Bombyx Mori* Silk. *Mater. Sci. Eng., C* **2007**, *27*, 675−683.

(38) Chen, S.; Liu, M.; Huang, H.; Cheng, L.; Zhao, H. P. Mechanical Properties of *Bombyx Mori* Silkworm Silk Fibre and Its Corresponding Silk Fibroin Filament: A Comparative Study. *Mater. Des.* **2019**, *181*, No. 108077.

(39) Abdel-Ghani, N. T.; El-Chaghaby, G. A.; Helal, F. S. Individual and Competitive Adsorption of Phenol and Nickel onto Multiwalled Carbon Nanotubes. *J. Adv. Res.* **2015**, *6*, 405−415.

(40) Ali, S.; Shah, I. A.; Ahmad, A.; Nawab, J.; Huang, H.; Ali, S.; Shah, I. A.; Ahmad, A.; Nawab, J.; Huang, H. Ar/O2 Plasma Treatment of Carbon Nanotube Membranes for Enhanced Removal of Zinc from Water and Wastewater: A Dynamic Sorption-Filtration Process. *Sci. Total Environ.* **2019**, *655*, 1270−1278.

(41) Wang, J. T.; Li, L. L.; Zhang, M. Y.; Liu, S. L.; Jiang, L. H.; Shen, Q. Directly Obtaining High Strength Silk Fiber from Silkworm by Feeding Carbon Nanotubes. *Mater. Sci. Eng., C* **2014**, *34*, 417−421.

(42) Wang, J. T.; Li, L. L.; Feng, L.; Li, J. F.; Jiang, L. H.; Shen, Q. Directly Obtaining Pristine Magnetic Silk Fibers from Silkworm. *Int. J. Biol. Macromol.* **2014**, *63*, 205−209.

(43) Lee, K. I.; Wang, X.; Guo, X.; Yung, K. F.; Fei, B. Highly Water-Absorbing Silk Yarn with Interpenetrating Network via in Situ Polymerization. *Int. J. Biol. Macromol.* **2017**, *95*, 826−832.

(44) Xu, H.; Yi, W.; Li, D.; Zhang, P.; Yoo, S.; Bai, L.; Hou, J.; Hou, X. Obtaining High Mechanical Performance Silk Fibers by Feeding Purified Carbon Nanotube/Lignosulfonate Composite to Silkworms. *RSC Adv.* **2019**, *9*, 3558−3569.

(45) Ayutsede, J.; Gandhi, M.; Sukigara, S.; Micklus, M.; Chen, H. E.; Ko, F. Regeneration of *Bombyx Mori* Silk by Electrospinning. Part 3: Characterization of Electrospun Nonwoven Mat. *Polymer* **2005**, *46*, 1625−1634.

(46) Chen, H.; Hu, X.; Cebe, P. Thermal Properties and Phase Transitions in Blends of Nylon-6 with Silk Fibroin. *J. Therm. Anal. Calorim.* **2008**, *93*, 201−206.

(47) Hu, X.; Kaplan, D.; Cebe, P. Determining Beta-Sheet Crystallinity in Fibrous Proteins by Thermal Analysis and Infrared Spectroscopy. *Macromolecules* **2006**, *39*, 6161−6170.

(48) Tulachan, B.; Meena, S. K.; Rai, R. K.; Mallick, C.; Kusurkar, T. S.; Teotia, A. K.; Sethy, N. K.; Bhargava, K.; Bhattacharya, S.; Kumar, A.; Sharma, R. K.; Sinha, N.; Singh, S. K.; Das, M. Electricity from the Silk Cocoon Membrane. *Sci. Rep.* **2014**, *4*, No. 5434.

(49) Alamusi, Hu. N.; Fukunaga, H.; Atobe, S.; Liu, Y.; Li, J. Piezoresistive Strain Sensors Made from Carbon Nanotubes Based Polymer Nanocomposites. *Sensors* **2011**, *11*, 10691−10723.

(50) Sala de Medeiros, M.; Goswami, D.; Chanci, D.; Moreno, C.; Martinez, R. V. Washable, Breathable, and Stretchable e-Textiles Wirelessly Powered by Omniphobic Silk-Based Coils. *Nano Energy* **2021**, *87*, No. 106155.

(51) Paredes-Madrid, L.; Palacio, C. A.; Matute, A.; Parra Vargas, C. A. Underlying Physics of Conductive Polymer Composites and Force Sensing Resistors (FSRs) under Static Loading Conditions. *Sensors* **2017**, *17*, 2108.

(52) Cheng, W.; Fu, J.; Hu, H.; Ho, D. Interlayer Structure Engineering of MXene-Based Capacitor-Type Electrode for Hybrid Micro-Supercapacitor toward Battery-Level Energy Density. *Adv. Sci.* **2021**, *8*, No. 2100775.

(53) Jiao, S.; Zhou, A.; Wu, M.; Hu, H. Kirigami Patterning of MXene/Bacterial Cellulose Composite Paper for All-Solid-State Stretchable Micro-Supercapacitor Arrays. *Adv. Sci.* **2019**, *6*, No. 1900529.

(54) Guo, C.; Zhang, J.; Wang, X.; Nguyen, A. T.; Liu, X. Y.; Kaplan, D. L. Comparative Study of Strain-Dependent Structural Changes of Silkworm Silks: Insight into the Structural Origin of Strain-Stiffening. *Small* **2017**, *13*, No. 1702266.

(55) Ye, C.; Ren, J.; Wang, Y.; Zhang, W.; Qian, C.; Han, J.; Zhang, C.; Jin, K.; Buehler, M. J.; Kaplan, D. L.; Ling, S. Design and Fabrication of Silk Templated Electronic Yarns and Applications in Multifunctional Textiles. *Matter* **2019**, *1*, 1411−1425.

(56) Zhai, S.; Karahan, H. E.; Wei, L.; Qian, Q.; Harris, A. T.; Minett, A. I.; Ramakrishna, S.; Ng, A. K.; Chen, Y. Textile Energy Storage: Structural Design Concepts, Material Selection and Future Perspectives. *Energy Storage Mater.* **2016**, *3*, 123−139.